Particle size effect of silver nanoparticles decorated single walled carbon nanotube electrode for supercapacitors

Chowdari, Bobba V. R.; Mak, Wai F.; Reddy, M. V.; Mhaisalkar, Subodh G.; Wee, Grace; Phonthammachai, Nopphawan; Kiebele, Andreas; Gruner, George; Srinivasan, Madhavi

2009

Wee, G., Mak, W. F., Phonthammachai, N., Kiebele, A., Reddy, M. V., Chowdari, B. V. R., et al. (2010). Particle size effect of silver nanoparticles decorated single walled carbon nanotube electrode for supercapacitors. Journal of the electrochemical society, 157(2). A179-A184.

https://hdl.handle.net/10356/102028

https://doi.org/10.1149/1.3267874

Journal of The Electrochemical Society, **157** (2) A179-A184 (2010)
0013-4651/2009/157(2)/A179/6/$28.00 © The Electrochemical Society

Particle Size Effect of Silver Nanoparticles Decorated Single Walled Carbon Nanotube Electrode for Supercapacitors

Grace Wee,[a] Wai F. Mak,[a] Nopphawan Phonthammachai,[a] Andreas Kiebele,[a] M. V. Reddy,[b] B. V. R. Chowdari,[b] George Gruner,[c] Madhavi Srinivasan,[a,z] and Subodh G. Mhaisalkar[a,z]

[a]*School of Materials Science and Engineering, Nanyang Technological University, Singapore 639798*
[b]*Department of Physics, National University of Singapore, Singapore 117542*
[c]*Physics and Astronomy Department, University of California, Los Angeles, California 90024, USA*

Well dispersed silver nanoparticles (AgNPs) of different sizes (1–13 nm) on single walled carbon nanotubes (SWCNTs) were synthesized by a facile room-temperature deposition–precipitation process. The morphology and microstructure of samples examined by the transmission electron microscopy showed a monodispersed silver particle decorated SWCNT of 2 wt % as determined by the Rietveld phase analysis of powder X-ray diffraction patterns. The chemical state of silver determined from the binding energies of high resolution Ag 3d peaks from X-ray photoelectron spectroscopy revealed a silver (Ag^0) oxidation state. Electrochemical properties were studied using cyclic voltammetry, galvanostatic charge/discharge, and electrochemical impedance studies. Silver decorated SWCNTs demonstrated to be effective bifunctional charge collectors and active electrode materials for a supercapacitor, exhibiting a higher specific capacitance (106 F g^{-1}) compared to pristine SWCNT (47 F g^{-1}). An enhancement observed with AgNP decoration is highly size-dependent and is related to the improved intertube contact resistance, electroactive surface considerations, as well as the participation of Ag in a faradaic reaction induced pseudocapacitance. Decorating the SWCNT with 1 nm AgNP doubled the energy density of the device, which on charge–discharge cycling retained 84% of the initial capacitance at the end of 8000 cycles.
 [DOI: 10.1149/1.3267874]

Manuscript submitted July 6, 2009; revised manuscript received October 19, 2009. Published December 15, 2009.

Supercapacitors with high power densities (~10 kW kg^{-1}), moderate energy densities (~5 Wh kg^{-1}), and long cycle life ($\gg 10^4$ cycles)[1] represent an important segment of charge storage devices for applications ranging from consumer electronics to green-energy harnessing and hybrid electric vehicles. While conventional supercapacitors comprise highly porous carbon and metallic charge collectors, carbon nanotubes (CNTs) have been explored as electrode materials for supercapacitors[2-5] and Li-ion batteries[6,7] due to their high electrical/thermal conductivity, chemical stability, low mass density, and large surface area.[8] Recently, we proposed an architecture comprised of a single layer dense CNT network as both a current collector and an active material,[9] which led to light-weight, flexible supercapacitors that also offer the opportunity for a roll-to-roll printing process. This "printed power" solution now addresses a critical gap in the deployment of printed electronics with printed supercapacitors potentially integrated with applications such as radio-frequency identification tags, wearable electronics, and backplanes for large-area displays, among others. Although the device architecture[9] is promising, the electrode performance needs further development to be comparable to existing carbon and current collector based supercapacitor electrodes.

In this work, we report optimization of the proposed CNT device architecture in terms of improvement in the energy density and device internal resistance (iR), which attributed to an electrode–electrolyte or intertube (CNT-CNT) contact resistance among others that limits the power density and charge–discharge capability of supercapacitors.[10-12] Strategies to overcome these may include coating with conducting polymers, amorphous carbon, or the use of metallic nanoparticles. It has been reported by Tanahashi[13] that a capacitance enhancement of about 300% was achieved by incorporating Ag particles into activated carbon fiber cloth electrodes for supercapacitors. However, the charge–discharge capability of the device was degraded after the cycling test due to the formation of dendrites. Looking at these promising properties of Ag, this paper reports an approach to use silver-nanoparticle decorated carbon nanotubes (Ag-CNTs) by a facile room-temperature deposition–precipitation (DP) process with the aim of reducing device iR and concurrently enhancing the device energy density. Galvanostatic studies, electrochemical impedance spectroscopy (EIS), and sheet resistance measurements suggest that the enhancement seen with silver nanoparticles (AgNPs) is highly size-dependent and is related to the improved intertube contact resistance, electroactive surface considerations, as well as the participation of Ag in a faradaic reaction induced pseudocapacitance.

[z] E-mail: madhavi@ntu.edu.sg; subodh@ntu.edu.sg

Experimental

Synthesis.— Silver decorated single walled carbon nanotube (SWCNT) (Ag-CNT) was prepared by first dispersing 0.8 g of SWCNT in 15 mL of deionized water followed by 20 min ultrasonication (120 kW). The SWCNT used here was P3-SWNT (Carbon Solution Inc.), which was purified using nitric acid, resulting in highly functionalized nanotubes (1.5–3 atom % carboxylic acid). Typically, this was done by refluxing CNTs in concentrated nitric acid (2–3 M) for 45 h.[14,15] The size of the AgNP was controlled through pH adjustment ($4 < pH < 7$) using 0.1 M NaOH (99%, Merck) that was added to 100 mL aliquots of $AgNO_3$ (99.99%, Aldrich, 0.05–0.15 M). The SWCNT suspension was mixed with the pH adjusted $AgNO_3$ solution and stirred vigorously for different time (15–120 min), yielding different AgNP sizes. The Ag-CNTs were separated by a centrifugation (15,000 rpm, 10 min), and excess Na ion and nitrate were removed by multiple washing steps with deionized water. The final product was then redispersed in deionized water before use.

Characterization.— Ag-CNT was characterized by transmission electron microscopy (TEM, JEOL 2100F) in a high resolution mode operating at 200 kV and by X-ray diffraction (XRD) using a Shimadzu diffractometer (Cu Kα) by step scanning (0.02°, 0.6 s dwell time) over a 10–140° 2θ range. The patterns were analyzed by the Rietveld method[16,17] using the fundamental parameter approach[18] contained within the software TOPAS V3 (Bruker-AXS). X-ray photoelectron spectroscopy (XPS) spectra were recorded using a Kratos AXIS Ultra spectrometer with the monochromatic Al Kα X-ray radiation. Deconvolution and peak fitting were performed with computer assisted surface analysis XPS software[19] using a Voigt function with 30% Lorentzian character and a Shirley background.

Electrode fabrication.— SWCNT or Ag-CNT suspension (0.2 mg mL^{-1} in deionized water) was filtered through a filter membrane (Whatman, 20 nm pore size, 47 mm diameter). The CNT

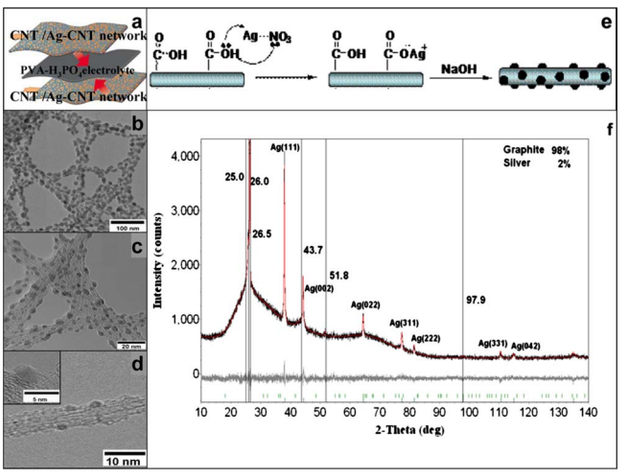

Figure 1. (Color online) (a) Schematic representation of the experimental cell assembly of the flexible supercapacitor. TEM images for (b) 13 ± 1, (c) 4 ± 1, and (d) 1 nm Ag-CNTs, with the inset showing a AgNP of ~1 to 2 nm decorated on the CNT. (e) Schematic representation of the AgNP decoration SWCNT surface. (f) Representative Rietveld phase analysis plot of Ag-CNT, showing metallic silver reflections and the weight percentage of AgNP on SWCNT.

(pristine or Ag decorated) was trapped on the surface of the filter, forming an interconnected network. After drying, the freestanding CNT network film (thickness of ≈20 μm) was peeled off from the filter and used as the electrode.

Electrolyte and supercapacitor device fabrication.— The acidic polymer electrolyte was prepared by heating 5 g of poly(vinyl alcohol) (PVA) monomer (Alfa Aesar, 98–99%, medium/high molecular weight) in 50 mL deionized water at 90°C to obtain a clear gel-like solution to which 3 mL of H_3PO_4 (Sigma-Aldrich, 85% purity) was added under continuous stirring. Air bubbles and excess water in the gel-like solution were removed using a vacuum desiccator and heating to 60°C for 4 h respectively, to obtain a polymer electrolyte film (0.5 mm thickness) that also acts as the separator between the two electrodes. Supercapacitor devices were fabricated by stacking this polymer electrolyte film in between two electrode strips of pristine or Ag-CNT, which were secured onto a poly(ethylene terephthalate) substrate using a double-sided adhesive tape (Fig. 1a).

Electrochemical studies.— Cyclic voltammetry (CV) and galvanostatic charge/discharge (GCD) cycle measurements were carried out in a two electrode configuration using a computer controlled bipotentiostat (Pine Instrument, AFBP1) in the potential range of 0–1 V (scan rate of 20 mV s^{-1}) and at a constant current density of ~1 mA cm^{-2}, respectively. AC impedance was measured at room temperature using an impedance spectrum analyzer (Solatron, SI 1255 impedance/gain-phase analyzer; computer software ZView) with an ac amplitude of 5 mV, from 55 kHz to 20 mHz at an open-circuit potential.

Results and Discussion

TEM images of Ag-CNT (Fig. 1b-d) revealed a uniform AgNP distribution on the SWCNT with the size varying from 1 to 13 nm. The DP method of $AgNO_3$ and NaOH was employed for the preparation of highly dispersed AgNP on CNTs, where the dispersion and size of AgNP are modified by adjusting the $AgNO_3$ concentration, pH, and aging time. The carboxyl groups (–COOH) on the CNTs act as the nucleation sites for silver deposition through the interaction with $AgNO_3$, forming $–COO^- Ag^+$ groups (Fig. 1e). With both carboxyl groups and hydroxyl ions which act as the reducing agents and accelerators in reduction synthesis,[20-23] Ag^+ could be in situ reduced to Ag^0 and evenly loaded on the –COOH functionalized CNT as reported elsewhere.[24,25] When the hydroxyl ions (OH^-) are sufficient for accelerating reduction (pH 4.3), there is high nucleation at the carboxyl groups and rapid growth of large silver crystals. The crystal sizes of AgNP became progressively smaller at higher pH (6 and 10 nm at pH 6.3 and 7.3) due to the reaction between excess hydroxyl ions and silver ions in the suspension that favors the formation of AgOH and prevents the growth of nucleated silver metals. The smallest crystals (1 nm) were obtained at the lowest concentration (0.05 M). For constant pH and silver concentrations, the smallest crystals were produced at the shortest aging time (15 min). The presence of AgNP on the SWCNT was further analyzed by the powder XRD, which showed diffraction peaks at $2\theta = 38$, 45, 64, 78, and 82° in addition to CNT,[26,27] confirming the formation of cubic Ag^0 nanoparticles on CNT (Fig. 1f). The amount of the loaded AgNP on the SWCNT was constant, as verified by the Rietveld phase analysis of powder XRD patterns, and the crystalline diffraction peaks revealed the AgNP amount as 2 wt % for all the samples.

Cyclic voltammograms for supercapacitors with bare-SWCNT (denoted as CNT) and Ag-CNT electrodes of various AgNP sizes (denoted as 1–13 nm Ag-CNT) are presented in Fig. 2a. The specific capacitance of a conventional activated carbon electrode with a PVA/H_3PO_4 electrolyte is <10 F g^{-1} (result not shown here); however, the specific capacitance of a dense CNT network is 46 F g^{-1}, showing good agreement with literature values[28] and its CV curve shows the peak at 0.1 V, which can be attributed to oxygen containing functional groups.[3] Surfactants and impurities contributed by the CNT synthesis are thought to lead to the deviations from the box-shaped CV characteristics of an ideal supercapacitor.[28] These box-shaped CV curve deviations are also observed for 1 and 4 nm Ag-CNTs, which exhibit significantly larger specific capacitances of 106 and 68 F g^{-1}, respectively, compared to bare CNT. An increase in specific capacitance with the addition of AgNPs may be attributed to the fact that the AgNPs participate in a faradaic reversible redox

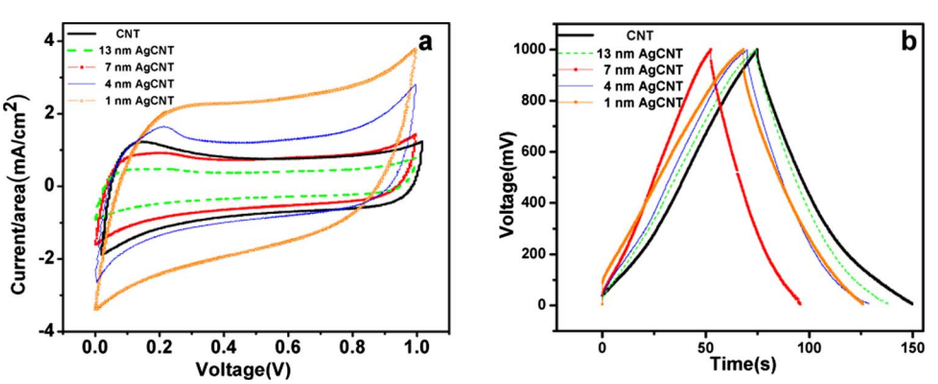

Figure 2. (Color online) (a) Cyclic voltammograms for CNT, 13 nm Ag-CNT, 7 nm Ag-CNT, 4 nm Ag-CNT, and 1 nm Ag-CNT devices measured at 20 mV s^{-1}. (f) Galvanostatic charge–discharge curves for the same devices mentioned in (a) measured at ~1 mA cm^{-2}.

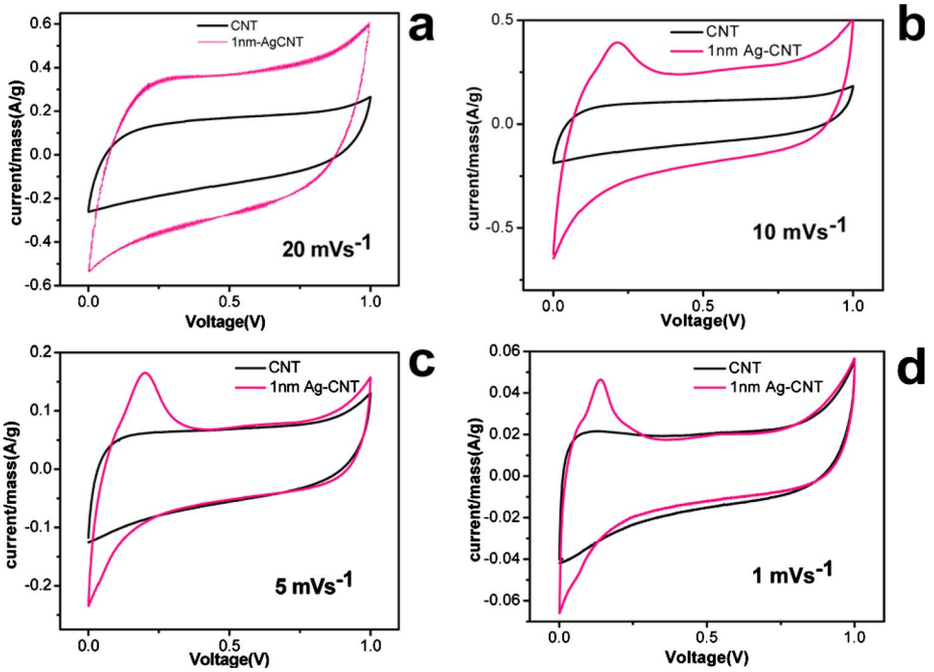

Figure 3. (Color online) Cyclic voltammogram curves for a pristine CNT and a 1 nm Ag-CNT electrode with a PVA/H_3PO_4 polymer electrolyte measured at different scan rates: (a) 20, (b) 10, (c) 5, and (d) 1 mV s^{-1}.

reaction leading to a pseudocapacitance contribution over and above the electrical double layer to the overall specific capacitance of the device.

To elucidate the mechanism of pseudocapacitance, cyclic voltammograms at different scan rates were collected for both pristine CNT and 1 nm Ag-CNT (Fig. 3). We observed obvious oxidation peaks for 1 nm Ag-CNT (Fig. 3b-d) at lower scan rates (<20 mV s^{-1}), which are absent in the CV curves of pristine CNT. As the reversible redox reaction is a diffusion-limiting process, the low scan rate allows enough time for charges to diffuse to the inner and less accessible active surface compared to the high scan rate which limits the accessibility of charges only to the outer active surface of the electrode.[29-31] Thus, the oxidation peaks, which can only be observed at lower scan rates for small AgNP decorated CNT, are a strong indication of the presence of pseudocapacitance compared to pristine CNTs, which only contribute to the electrical double layer capacitance. The higher the scan rate, the moderately lower the response from faradaic reactions, hence revealing that some diffusion and resistance limitation take place. CVs at different potential scan rates reveal that the peak potential shifts at a higher scan rate and the peak is not obvious at a high scan rate (Fig. 3a), which indicates that the exact mechanism of the pseudocapacitative behavior of silver is different from that of oxides and needs further investigation.[32,33] To evaluate the reversibility of the faradaic process, cycle stability of 1 nm Ag-CNT was investigated by the galvanostatic charge–discharge at a current density of 1 mA cm^{-2}, and the specific capacitance of the device after 8000 cycles was ~84% of its initial capacitance (Fig. 4b) that is attributed to the accompanying faradaic pseudocapacitance process. XPS studies of the 1 nm Ag-CNT electrode before charging (Fig. 5a) show the presence of silver in the Ag^0 oxidation state in the sample, as indicated from the binding energies (BEs) of Ag $3d_{5/2}$ and Ag $3d_{3/2}$ spin-orbit split peaks. After charging, in addition to these, additional peaks were observed at a higher BE, which may be attributed to silver oxides (Fig. 5b). The appearance of this additional peak after charging suggests that during charging of the electrode, some of the silver (Ag^0) take part in a reversible pseudocapacitative surface redox process getting converted to oxide ($Ag^0 \leftrightarrow Ag^+ + e^-$; $2Ag + 2OH^- \rightarrow Ag_2O + H_2O$).[24]

The specific capacitance decreases with increasing Ag particle size with 7 and 13 nm Ag-CNT devices, yielding values of 43 and 23 F g^{-1}, respectively. Similar observations were also obtained from the measurement of a specific capacitance using the GCD method, with the capacitance values (Fig. 2b and Table I) mirroring the CV results. The specific capacitance obtained for AgNP with a particle size greater than 4 nm was less than the bare SWCNT, indicating a pore blockage of the CNT network by the larger AgNP, resulting in

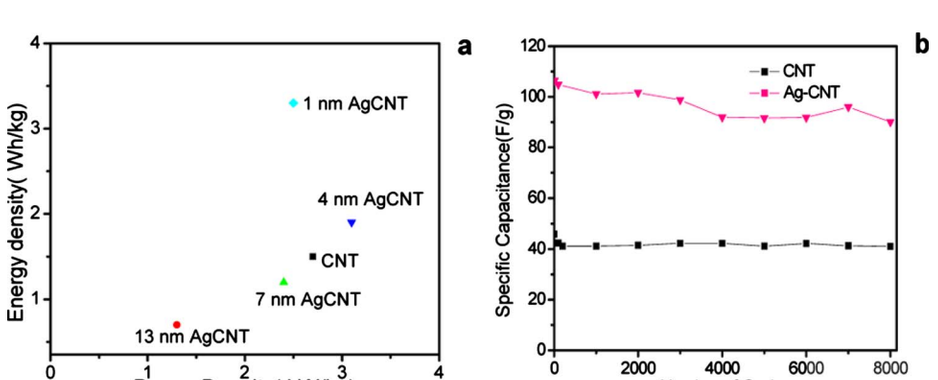

Figure 4. (Color online) (a) Ragone plot of supercapacitors consisting of Ag-CNT electrodes with PVA/H_3PO_4 electrolyte. (b) Cycle stability of a pristine CNT and a 1 nm Ag-CNT electrode with a PVA/H_3PO_4 polymer electrolyte with a charge–discharge current density of 1 mA cm^{-2}.

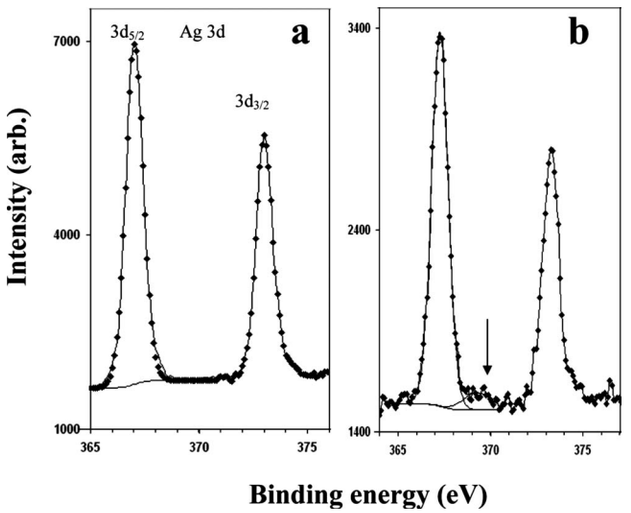

Figure 5. High resolution curve fitted Ag 3d X-ray photoelectron spectroscopic scan of 1 nm Ag-CNT (a) before and (b) after charging to 1 V.

a reduction in the electroactive surface for forming the electrical double layer. Smaller AgNPs (with diameter <5 nm) are less likely to block the CNT network pores and thus augment the formation of the electrical double layer. It is also important to note that the wetting behavior of a polymer and a liquid electrolyte is different, with the former wetting only the surface rather than the entire cross-sectional thickness of the electrode. The capacitance normalized by the area of the electrode (F/cm^2) has been evaluated for all the devices, with the values showing a similar trend as specific capacitance (F/g), as shown in Table I.

The effect of AgNP on the supercapacitor performance and the electrochemical behavior of Ag-CNT electrodes were further investigated with ac impedance spectroscopy (Fig. 6a). An equivalent circuit simulating Ag-CNT electrodes would involve the following circuit elements: the bulk solution resistance R_s, the double layer capacitance C_{dl}, the interfacial charge-transfer resistance R_{ct}, and the Warburg impedance due to the distributed resistance within the mesopores W_s. Because we have combined both active material and current collector into a single component in our devices, C_b and R_b correspond to the capacitance and resistance within the electrode. The combination of the circuit elements is proposed and shown in Fig. 6b and c, respectively. Accordingly, the overall impedance Z of the equivalent circuit for all devices without the presence of a pseudocapacitance is given by

$$Z = R_s + \frac{R_b}{j\omega R_b C_b + 1} + \frac{R_{ct}}{j\omega R_{ct} C_{dl} + 1} \quad [1]$$

Equation 1 is applied for obtaining the best-fit EIS curves of CNT, 13 and 7 nm Ag-CNT devices. However, for 1 and 4 nm Ag-CNTs in particular, an additional element of C_p, corresponding to the

Table I. Specific capacitance, iR, and sheet resistance measured in the PVA/H_3PO_4 electrolyte for all devices using both CV and GCD methods.

Sample	Area per electrode (cm^2)	Mass per electrode (mg)	C (F cm^{-2})		C (F g^{-1})		iR (Ω)	Sheet resistance (Ω □$^{-1}$)
			CV	GCD	CV	GCD		
P3CNT	0.6	1.10	0.09	0.08	46.5	41.9	83.2	15.7
13 nm Ag-CNT	0.6	1.20	0.05	0.03	22.8	16.5	159.9	10.3
7 nm Ag-CNT	0.7	1.40	0.09	0.06	43.4	28.3	72.8	5.9
4 nm Ag-CNT	0.5	1.23	0.15	0.10	67.5	44.8	65.5	6.3
1 nm Ag-CNT	0.5	1.22	0.24	0.21	105.8	89.4	83.0	10.2

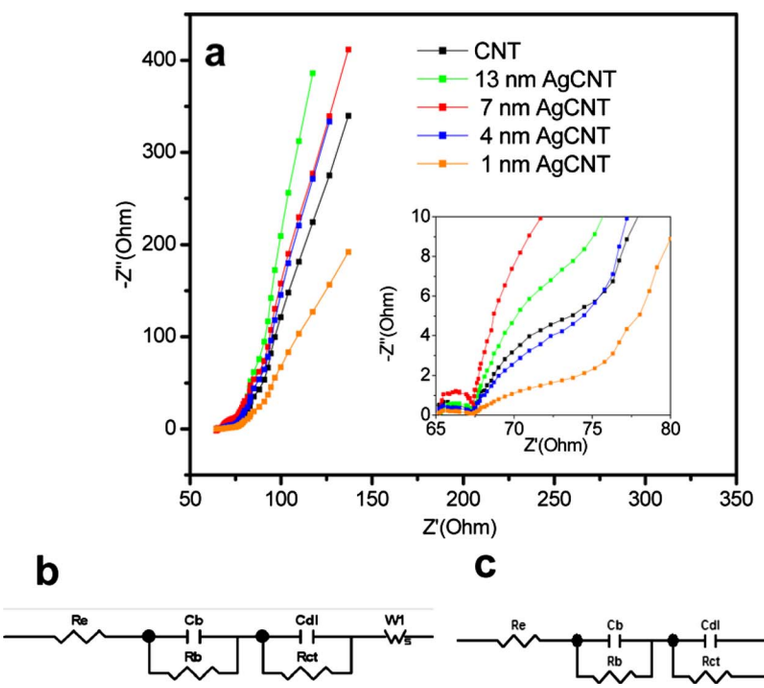

Figure 6. (Color online) (a) Nyquist impedance plots, inset showing the high frequency, low impedance region. (b) Equivalent circuit model for CNT, 13 nm Ag-CNT, and 7 nm Ag-CNT devices. (c) Equivalent circuit model for 4 and 1 nm Ag-CNT devices.

Table II. Components of the equivalent circuit fitted for the impedance spectra of all devices.

Sample	R_b (Ω)	R_{ct} (Ω)	C_t (μ F cm^{-2})	C_d (F cm^{-2})	$C_{dl} + C_p$ (F cm^{-2})
CNT	1.511	28.13	18.252	0.03	—
13 nm Ag-CNT	0.84	87.24	46.883	0.017	—
7 nm Ag-CNT	2.301	47.8	13.611	0.01	—
4 nm Ag-CNT	0.945	3.773	18.699	—	0.054
1 nm Ag-CNT	0.467	1.38	50.409	—	0.117

pseudocapacitance, was required in the equivalent circuit for the best-fitted EIS curves. The equation of the impedance with an additional element of a pseudocapacitance Z is expressed as

$$Z = R_s + \frac{R_b}{j\omega R_b C_b + 1} + \frac{1}{j\omega C_{dl} + \frac{j\omega C_p}{j\omega R_{ct} C_p + 1}} \quad [2]$$

By fitting Eq. 1 and 2 to the respective impedance data (Fig. 6a), the values shown in Table II have been evaluated.

The electrolyte resistance was approximately 65 Ω; this relatively higher value compared to the liquid electrolyte (<10 Ω)[34] is mainly due to the lower mobility of ions within the polymer electrolyte. The R_{ct} value for each Ag-CNT electrode accounts for a major proportion of the overall resistance, whereas R_b plays a minor role. The charge-transfer resistance R_{ct} decreases as the AgNP sizes become smaller, and a significant decrease is observed for 4 and 1 nm Ag-CNT devices, with R_{ct} in the range of 1–4 Ω (Table II). This observation indicates that AgNP in the size range of 1–5 nm effectively reduces the resistance between the CNT electrode and the electrolyte, whereas larger AgNPs (>7 nm) possibly reduce the electrochemical redox kinetics by blocking the pores on the CNT network surfaces, yielding R_{ct} values of 87 Ω for a 13 nm Ag-CNT device, significantly higher even than the reference CNT device (~ 28 Ω).

The double layer capacitance C_{dl} obtained from the impedance analysis increases as AgNP reduces from 7 to 1 nm, which agrees with the observation from the CV measurement. The pseudocapacitance C_p for 4 and 1 nm Ag-CNT devices contributed to the overall capacitance as $C_{dl} + C_p$. Again, 1 nm Ag-CNT has the highest capacitance among all the devices, further supporting the findings from CV measurements, which indicates that the pseudocapacitance is an important contributor to the enhancement of a capacitance for the <5 nm AgNP devices. The values of R_b and C_b (contribution from the electrodes) were negligibly small compared to the overall resistances and capacitances.

The low iR is of critical importance in supercapacitors because it is one of the limiting factors for power density ($P = V^2/4R$) and also influences the charge–discharge cycles. In supercapacitors, many sources contribute to the iR and are collectively measured and referred to as the equivalent series resistance (ESR).[8] Contributors to the ESR of supercapacitors include the sheet resistance of the electrode, the interfacial resistance between the electrode and the electrolyte, the ionic resistance of the electrolyte, and the external lead contact resistance.

The sheet resistance, as measured at several points on the network using a probe station, decreases from 15.7 Ω $\square^{-1}$ for the reference CNT device to lower values with a minimum sheet resistance of 5.9 Ω $\square^{-1}$ observed at a AgNP size of 7 nm (Table I). Because the CNT electrodes are well above the percolation threshold for nanotubes, the charge transport can be expected to be dominated by metallic conduction paths, and thus these results can be explained by two collaborating mechanisms. The addition of the AgNPs increases the percentage of a metallic material (AgNP plus metallic CNT) as opposed to the pure CNT where a ratio of a metallic CNT to a semiconducting CNT of 1:2 is expected. This leads to an increased number of metallic conduction paths and thus to a lower resistance due to the law of inverse addition of parallel resistances. Additionally, nanostructured silver possesses a lower resistivity than metallic CNTs,[35,36] which results in conduction paths that are partially or fully made up from silver having a smaller resistance.

The iRs of the capacitors were obtained using a GCD test (Fig. 2b). From the voltage drop at the beginning of the discharge curve, the iR of the CNT electrode was found to be 83.2 Ω. Incorporation of AgNP into the CNT network yields an iR of 65 Ω for 4 nm Ag-CNT; however, the 13 nm Ag-CNT device displays a high iR of 160 Ω. The result of both internal and sheet resistances of the electrode is shown in Table I, giving a clearer overview on the correlation between AgNP sizes and both the internal and sheet resistances of the devices.

To understand the observed behavior of the iR, the effect of Ag on the intratube as well as the intertube resistances of semiconducting CNTs needs to be discussed. Whenever a contact is formed between a metal and a semiconductor, Fermi level alignment is expected to occur, resulting in a charge redistribution and the formation of a depletion layer surrounding the metal. Thus, such phenomenon may contribute to the intratube resistance of the Ag-CNTs which creates a localized depletion region, acting as a charge scattering site and leading to a decrease in mobility and intratube conductivity. However, it may be argued that the depth of the depletion region increases with the number of atoms in the nanocluster, reaching a maximum value somewhere in the 5–20 nm range, beyond which this depth may remain constant.[37] The significant intertube contact resistance between semiconducting and metallic CNTs has been attributed to the creation of a Schottky barrier.[38] The semiconducting-metallic CNT junction mediated with Ag nanoparticles may lead to a reduction in the Schottky barrier height, thus reducing the intertube contact resistance. The superposition of these two effects could explain the observed size-dependent variation in the iR. With growing interest in nanoparticle decorated nanowires and conducting networks, the importance of characterizing intra- and intertube contact resistances need not be emphasized and constitutes ongoing investigations in our laboratories and in several laboratories worldwide.

The observations detailed in the preceding paragraphs may thus be summarized as follows: The specific capacitance in Ag-CNT supercapacitors comprised of contributions from the (*i*) nonfaradaic electrical double layer capacitance and (*ii*) faradaic pseudocapacitance from the silver surface redox reaction that is governed by the available electroactive surface strongly influenced by the AgNP size. Our studies show that the AgNP smaller than 5 nm augments the double layer formation by not blocking the CNT network, and in addition undergoes the surface redox reaction contributing to the pseudocapacitance, thus resulting in enhancement of the specific capacitance and energy density (106 F g^{-1} and 3.3 Wh kg^{-1}), which is twice as high compared to the pristine CNT (Table I and Fig. 4a). It is evident that by employing a device configuration without metal current collectors, the energy and power densities of our supercapacitors are improved with Ag-CNT compared to pristine CNT electrodes,[9] and comparable to other studies using metal current collectors and decoration of CNTs with Ni nanoparticles[31] and transition-metal oxides such as RuO_2,[33] MnO_2,[39,40] SnO_2, and TiO_2.[41]

Conclusion

Ag-CNTs are demonstrated to be effective charge collectors and electrode materials for supercapacitors. The capacitance and energy density of the device can be doubled by decorating CNT with AgNP of ~1 nm, which do not block the CNT network and complement the double layer capacitance by a faradaic reaction induced pseudocapacitance. The iR of the device can also be reduced, and the power density is increased by utilizing the AgNP in the ~4 nm range. It should be noted that the simple methodologies presented herein may be readily extended to other metallic nanoparticles as well as decoration with suitable transition-metal oxide nanoparticles, which would further enhance the pseudocapacitance of the devices and render these hybrid electrode materials attractive candidates for both high load and printed power applications.

Nanyang Technological University assisted in meeting the publication costs of this article.

References

1. B. E. Conway, *Electrochemical Supercapacitors: Scientific Fundamentals and Technological Application*, Chap. 1, Kluwer Academic, Dordrecht/Plenum, New York (1999).
2. C. Niu, E. K. Sichel, R. Hoch, D. Moy, and H. Tennent, *Appl. Phys. Lett.*, **70**, 1480 (1997).
3. J. N. Barisci, G. G. Wallace, and R. H. Baughman, *J. Electroanal. Chem.*, **488**, 92 (2000).
4. S. Shiraishi, H. Kurihara, K. Okabe, D. Hulicova, and A. Oya, *Electrochem. Commun.*, **4**, 593 (2002).
5. C. G. Liu, H. T. Fang, F. Li, M. Liu, and H. M. Chenga, *J. Power Sources*, **160**, 758 (2006).
6. A. S. Claye, J. E. Fischer, C. B. Huffman, A. G. Rinzler, and R. E. Smalley, *J. Electrochem. Soc.*, **147**, 2845 (2000).
7. S. H. Ng, J. Wang, Z. P. Guo, J. Chen, G. X. Wang, and H. K. Liu, *Electrochim. Acta*, **51**, 23 (2005).
8. A. G. Pandolfo and A. F. Hollekamp, *J. Power Sources*, **157**, 11 (2006).
9. M. Kaempgen, G. Wee, J. Ma, S. G. Mhaisalkar, and G. Gruner, *Appl. Phys. Lett.*, **90**, 264104 (2007).
10. G. Gruner, *J. Mater. Chem.*, **16**, 3533 (2006).
11. E. Bekyarova, M. E. Itkis, N. Cabrera, B. Zhao, A. Yu, J. Gao, and R. C. Haddon, *J. Am. Chem. Soc.*, **127**, 5990 (2005).
12. A. Kiebele, M. Kaempgen, and G. Gruner, *Nanotechnology Law & Business*, **5**, 7 (2008).
13. I. Tanahashi, *Electrochem. Solid-State Lett.*, **8**, A627 (2005).
14. J. Liu, A. G. Rinzler, H. Dai, J. H. Hafner, R. K. Bradley, P. J. Boul, A. Lu, T. Iverson, K. Shelimov, C. B. Huffman, et al., *Science*, **280**, 1253 (1998).
15. A. G. Rinzler, J. Liu, H. Dai, P. Nikolaev, C. B. Huffman, F. J. Rodríguez-Macías, P. J. Boul, A. H. Lu, D. Heymann, D. T. Colbert, et al., *Appl. Phys. A: Mater. Sci. Process.*, **67**, 29 (1998).
16. H. M. Rietvield, *Acta Crystallogr.*, **22**, 157 (1967).
17. H. M. Rietveld, *J. Appl. Crystallogr.*, **2**, 65 (1969).
18. R. W. Cheary and A. Coelho, *J. Appl. Crystallogr.*, **25**, 109 (1992).
19. N. Fairley and A. Carrick, *The Casa Cookbook*, Pt. 1, Acolyte Science, Knutsford, Cheshire, UK (2005).
20. X. M. Sun and Y. D. Li, *Angew. Chem., Int. Ed.*, **43**, 597 (2004).
21. X. W. Pei, J. C. Hao, and W. M. Liu, *J. Phys. Chem. C*, **111**, 2947 (2007).
22. M. Singh, I. Sinha, and R. K. Mandal, *Mater. Lett.*, **63**, 425 (2009).
23. H. Wang, X. Qiao, J. Chen, and S. Ding, *Colloids Surf., A*, **256**, 111 (2005).
24. H. Yue, X. Huang, and Y. Yang, *Mater. Lett.*, **62**, 3388 (2008).
25. H. X. Chao, R. J. Zhou, M. M. Shi, Y. Gao, G. Wu, X. B. Zhang, H. Z. Chen, and M. Wang, *Nanotechnology*, **19**, 325605 (2008).
26. P. C. Ma, J. K. Kim, and B. Z. Tang, *Electronic Materials and Packaging (EMAP)*, **2006**, 1 (2006).
27. A. Zamudio, A. L. Elias, J. A. Rodriguez-Manzo, F. Lopez-Urias, G. Rodriguez-Gattorno, F. Lupo, M. Ruhle, D. J. Smith, H. Terrones, D. Diaz, et al., *Small*, **2**, 346 (2006).
28. E. Frackowiak and F. Beguin, *Carbon*, **39**, 937 (2001).
29. J. Yan, Z. Fan, T. Wei, J. Cheng, B. Shao, K. Wang, L. Song, and M. Zhang, *J. Power Sources*, **194**, 1202 (2009).
30. P. Soudan, J. Gaudet, D. Guay, D. Belaner, and R. Schulz, *Chem. Mater.*, **14**, 1210 (2002).
31. J. Wang, J. Polleux, J. Lim, and B. Dunn, *J. Phys. Chem. C*, **111**, 14925 (2007).
32. I. Kim, J. Kim, B. Cho, Y. Lee, and K. Kim, *J. Electrochem. Soc.*, **153**, A989 (2006).
33. I. Kim, J. Kim, and K. Kim, *Electrochem. Solid-State Lett.*, **8**, A369 (2005).
34. C. T. Hsieh, Y. W. Chou, and W. Y. Chen, *J. Solid State Electrochem.*, **12**, 663 (2008).
35. Y. Sun, B. Gates, B. Mayers, and Y. Xia, *Nano Lett.*, **2**, 165 (2002).
36. T. W. Ebbesen, H. J. Lezec, H. Hiura, J. W. Bennett, H. F. Ghaemi, and T. Thio, *Nature (London)*, **382**, 54 (1996).
37. D. R. Kauffman and A. Star, *Nano Lett.*, **7**, 1863 (2007).
38. M. S. Fuhrer, J. Nygard, L. Shih, M. Forero, Y. G. Yoon, M. S. C. Mazzoni, H. J. Choi, J. Ihm, S. G. Louie, A. Zettl, et al., *Science*, **288**, 494 (2000).
39. V. Subramanian, H. Zhu, and B. Wei, *Electrochem. Commun.*, **8**, 827 (2006).
40. S. L. Chou, J. Z. Wang, S. Y. Chew, H. K. Liu, and S. X. Dou, *Electrochem. Commun.*, **10**, 1724 (2008).
41. A. L. M. Reddy and S. Ranaprabhu, *J. Phys. Chem. C*, **111**, 7727 (2007).